Comparison of Predictions from a Ray Tracing Microcellular Model with Narrowband Measurements

G.E.Athanasiadou, A.R.Nix and J.P.McGeehan

Centre for Communications Research, University of Bristol,
Merchant & Venturers Building, Woodland Road, Bristol BS8 1UB, UK.
Fax: +44 (0)117 9545206, Tel. +44 (0) 117 9545203,
E-mail: G.Athanasiadou@bristol.ac.uk

Abstract: **In this paper predictions from a 3-D 'image-based' ray tracing model for microcellular environments are compared with three sets of narrowband measurements performed in a typical urban area. The comparisons illustrate that good agreement can be obtained, with RMS errors less than 3.7dB, even for deep shadow areas. In order to analyse the inherent discrepancies that result from the limited averaging of the measurements along the route, predictions were also obtained by producing slow fading envelopes similar to those measured.**

I. INTRODUCTION

Due to the site specific nature of microcellular environments, propagation models are required to take into account the exact position, orientation and electrical properties of individual buildings. In recent years, ray tracing has emerged as a viable technique for producing deterministic channel models based on the processing of user-defined environments. Such models can be used to obtain sets of results that may be impractical or too costly to obtain by measurements. These new simulation tools will enable researchers and designers to accurately predict the performance of wireless systems under a wide range of conditions [1]. As cell sizes reduce, the need to accurately plan basestation locations will become critical due to a need to minimise infrastructure costs.

The ray tracing algorithm used here [2-3] is based on the theory of images [4-5] and allows the rapid generation of complex channel impulse response characteristics for any given location of transmitter and receiver. The model makes full use of reflection, transmission and diffraction and, with sufficient memory, can evaluate scenarios incorporating many thousands of objects. Previous models [4-8] have been 2D or 3D in nature. In this model a hybrid technique is applied where the object database is held in two dimensions but the ray-tracing engine operates in three dimensions. The base station and the mobiles are assumed to remain below roof top height and based on this assumption, the buildings are modelled as infinitely tall. Although the building database is two dimensional, the model generates a 3D environment by specifying the antenna heights. Since the transmitter and receiver are stored using 3-D co-ordinates, the plane of the ray can be calculated and all reflections, transmissions and diffractions computed using 3-D vector mathematics (Figure 1). This hybrid analysis allows factors such as polarisation and 3D antenna patterns to be fully considered in the model. For each path found in the image tree, an additional ray is created corresponding to its ground reflection. For a more detailed description of the model, see reference [2].

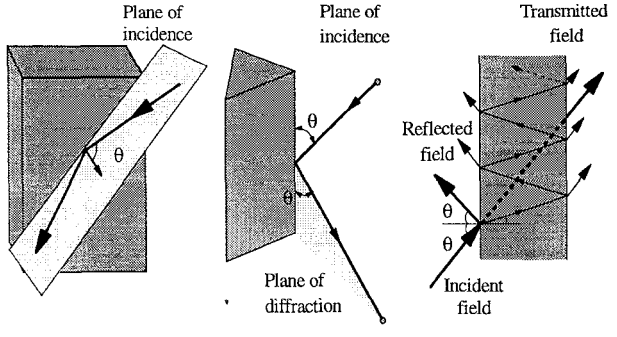

Figure 1: Propagation primitives

II. MEASUREMENT SET UP

In order to evaluate the power predictions of the model, simulation results are compared with narrowband measurements taken in a typical urban area, in central Bristol, UK. The field trials were performed under the British Telecom VURI project [9]. The measurement site, shown in Figure 2, is a well developed urban area with multi-storey buildings, hence the transmitter, as well as the receiver, is below the roof height of adjacent buildings. The transmitting antenna was on a mast at a height of 5m above ground level. The transmitter was used in CW mode

0-7803-3659-3/97 $10.00 ©1997 IEEE

at a frequency of 1.823GHz and the transmitted power for all the tests was 30dBm (including the cable and antenna losses). The receiver was at a height of 1.57m, mounted on a trolley which was slowly and carefully moved along the predefined route shown in Figure 2. The trolley was used instead of a car in order to increase the accuracy of the mapping of the measurement results to actual positions, which is critical when validating site specific models. Typical half wavelength vertically polarised dipoles were used at both ends of the link.

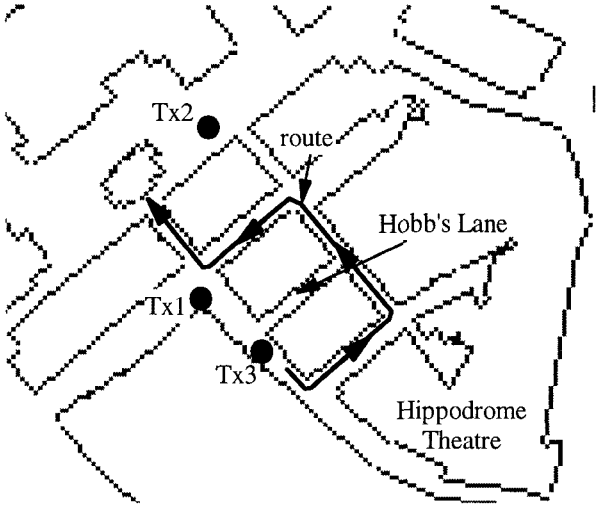

Figure 2: Microcellular map of the measurement area.

The narrowband receiver used for the measurements recorded field strength against distance from the starting point, with a spatial sampling rate of 4cm. The fast fading of each measurement was extracted with a rectangular sliding window averaging process. A 10 wavelength window was chosen, (equivalent to 1.67m), so that the measurements maintain their site specific information as much as possible.

The model's performance is evaluated under NLOS, as well as LOS conditions. Most importantly, the route includes deep shadow areas where energy can reach the receiver only through multiple reflected and diffracted rays. Field trials were carried out along the same route for three different transmitter positions. For each transmitter location, several measurement runs (three to six) were performed along the same route and with the same configuration. For more representative results (in order to remove localised temporal effects), the slow fading envelopes were averaged to produce a mean envelope.

III. Model Set up

For ray tracing to be used in practical situations the model must be capable of importing standard building databases. The Bristol building data was extracted from the UK Ordnance survey 'Landline' database. The map was then pre-processed to remove any redundant information and diffraction corners were automatically added. The simulated area is approximately 500x500m^2 and contains 438 walls (Figure 3). All buildings were modelled with the same electrical properties (ε_r=5, σ=0.005 Sm^{-1}), similar to those used in other studies (e.g. [2, 6]). The walls were assumed smooth and to have a thickness of 0.4m. For the results shown here, all rays were traced up to seven orders of reflection and two orders of diffraction. All predictions were obtained with the same simulation parameters.

Unlike the field trials, the space resolution between the prediction points was 0.5m. This is because the predicted received power which is produced as the sum of the power of the rays reaching the receiver, is inherently time averaged and no further action is needed to remove the fast fading. Nevertheless, spatial averaging can also be used in order to reduce the uncertainty that the chosen prediction point is a special case (this is particularly important in indoor environments [10]).

Predictions emulating the measurement process

A second set of predictions were produced from the model by emulating the measurement process. From the complex channel impulse responses, the 'instantaneous' power was produced every 4cm. At each point, the summation of the complex fields of all the rays reaching the receiver produces the total field strength from which the power prediction derives. The predictions obtained in this manner are equivalent to the raw data of a measurement run. Following the averaging process used for the measurements, a 10 wavelength sliding window was used to remove the fast fading and produce the slow fading envelope. Four such envelopes were produced. Because of the completely static environment of a ray tracing model, for each new envelope the starting point of the route was randomly offset to produce a different envelope. Alternatively, random phases could be used but the spatial offsets were preferred in order to reduce the receiver position uncertainty. The slow fading envelopes were then averaged to produce a mean predicted envelope similar to the measured envelope.

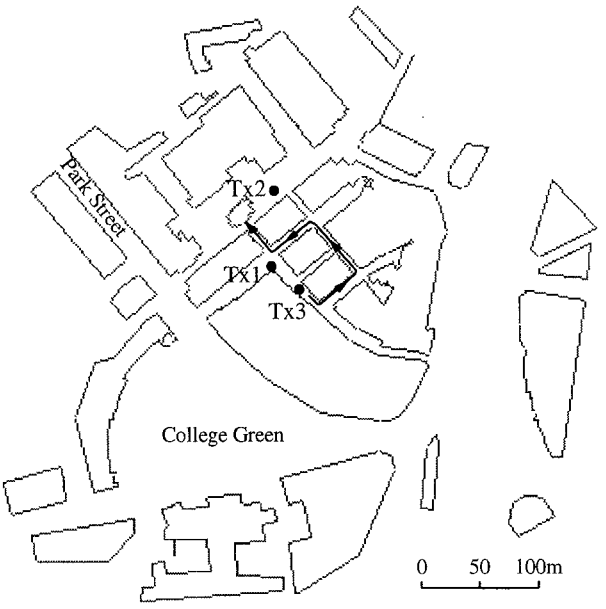

Figure 3: The model's building database.

IV. Comparison Between Measurements and Predictions

1. First transmitter position, Tx1:

Figure 4 depicts the mean measured envelope for the first transmitter position, Tx1, along with the model's prediction. At the beginning of the route the receiver is in a LOS position about 50m away from the transmitter. As it turns left and moves into NLOS positions, the mean signal level decreases significantly (more than 20dB, at ~20m). A further drop (less than 10dB, at ~60m) is evident as the receiver turns into the second corner and enters a deep shadow region. An increase of at least 18dB in power is due to the movement of the receiver along the end of Hobb's Lane (see Figure 2) which acts as a street canyon for the transmitted electromagnetic waves (~86m). As the receiver re-enters the deep shadow area, the power falls again, however higher signal levels are measured since the distance between the two antennas is smaller. When the receiver turns left and enters less shadowed areas (~118m) the signal increases by about 15dB and keeps increasing as the trolley approaches the second LOS section of the route. The transition from NLOS to LOS (~157m) is not as dramatic (approximately 10dB increase) because the two antennas were already very close and strong reflections had risen the mean signal strength. The measured power falls slowly as the receiver moves away from the transmitter and finally re-enters a NLOS area near the end of the route. Obviously, because the power changes are site dependent, there is no simple rule for the degree of variation of the signal level as the receiver moves into or out of LOS or NLOS or deep shadow areas.

As seen in Figure 4, the simulation results agree well with the measurement trend throughout the route, remaining within a few dB from the mean measurement for the majority of the receiver positions. When the calculations are performed with linear values and normalisation to the measured samples, the mean error is -1.3dB and the RMS error is 3dB. The mean difference between the predictions and the measurements, calculated with both values in a logarithmic scale, is just 1dB with an RMS error of 3.2dB.

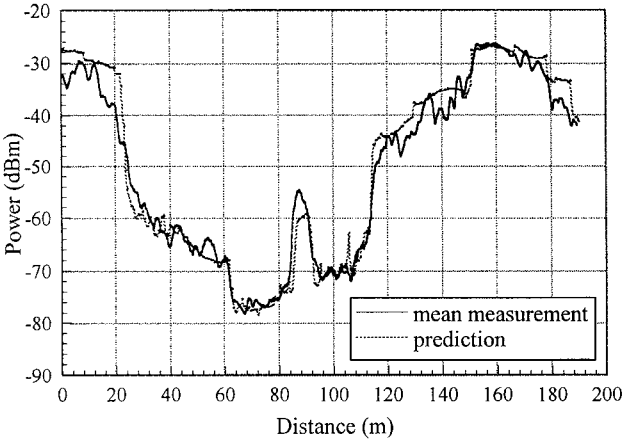

Figure 4: Model's prediction against mean measurement for the first transmitter position, Tx1.

1.1 Predictions emulating the measurement process

The mean prediction that is produced by averaging the simulated envelopes, varies more than the model's prediction calculated from the summation of the powers of the rays, as seen in Figure 4 and Figure 5. Although, there is only a small difference between the model's predictions with the two different averaging methods, the prediction with the averaged samples keeps better track of the mean measurement, as shown in Figure 5. Furthermore, the fluctuations of the mean simulated envelope are very similar to those of the measured envelope. Because each envelope point derives from spatial averaging along 10 wavelengths, the predicted envelopes, like the measurements, do not present sudden peaks similar to those appearing at the point prediction (see Figure 4 at ~105m). As seen in Figure 4 and Figure 5, as the receiver turns into the first corner, at about 20m away from the route start, the transition from the LOS to NLOS area is more abrupt for the simulation results rather than the

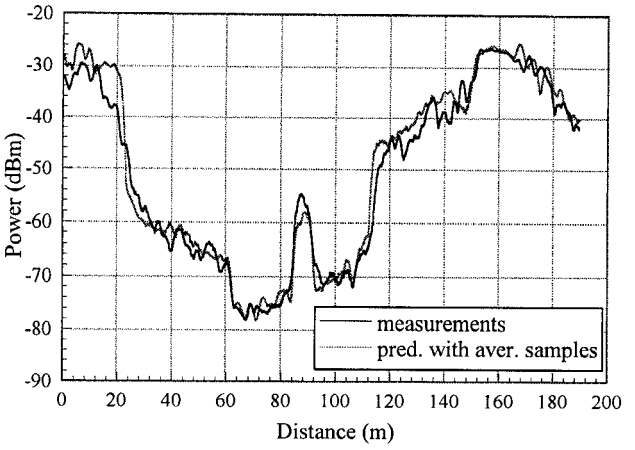

Figure 5: Model's prediction produced with averaged samples and the mean measurement for transmitter Tx1.

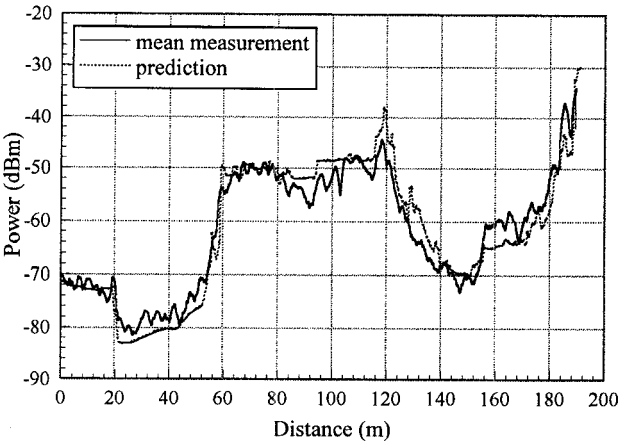

Figure 6: Model's prediction against mean measurement for transmitter position Tx2.

measurements. It is believed that missing scatterers in the database caused this divergence.

The error statistics are slightly better for the prediction with the averaged samples than with the prediction of the summation of the power of the rays. When the calculations are performed with linear values normalised to the measured samples, the mean error is –2.3dB and the RMS error is 2.4dB. The mean difference between the averaged predicted and measured envelopes, calculated with both values in a logarithmic scale, is just 0.7dB with an RMS error of 3dB.

2. Second transmitter position, Tx2:

As shown in Figure 2, the second transmitter position, Tx2, is outside the immediate area of the measurement route with LOS only in the last 1m of the route. This location was chosen in order to ensure that a large portion of the route is in the shadow region with respect to the transmitter. For this position, three measurement runs were performed. Figure 6 depicts the mean measurement for Tx2, together with the model's predictions (sum of the powers of the rays). During the first 50m of the route the received signal level is relatively low since there are three buildings between the two antennas. As the trolley turns into the second corner the received power increases by more than 20dB (~60m), as rays can now easily reach the receiver by travelling along the road which acts as a waveguide. A significant decrease in signal power (about 25dB) is caused as the receiver turns into the third corner, (~118m). Although the received power increases by about 10dB as the receiver turns into the last corner (~157m), the signal remains low as long as the trolley is behind the building and only at the last section of the route, as the receiver approaches the LOS area, does the signal level start increasing again.

Despite the difficulty of this route, which lies almost entirely in the NLOS area, the model manages to keep very good track of the measurements even in deep shadow areas, 100m away from the transmitter. The error statistics of the prediction are also very good. When the values are expressed in a linear scale, the normalised to the measurements mean error is –4.6dB, with an RMS error of 1.1dB. The mean difference between the predictions and the measurements, calculated with both values in a logarithmic scale, is -0.02dB and the RMS error is 3.3dB.

3. Third transmitter position, Tx3:

The third transmitter location, Tx3, is the one closest to the measurement route, as seen in Figure 2. By placing the transmitter at this position, the deep shadowing encountered along the route for both previous transmitter locations has been reduced. Figure 7 depicts the mean measurement produced from the four measurement runs performed. The shape of the measured envelope is similar to the measured envelope for Tx1 (see Figure 4), however with different power levels. During the first LOS section of the route, the measured power is about 10dB higher than that for Tx1. As the receiver enters the NLOS region, the signal falls significantly, more than 20dB. Unlike when the transmitter was at position Tx1, as the receiver turns around the second corner, the power level does not change dramatically because strong reflected and diffracted rays can still reach the receiver travelling around the building between the two antennas. As the power starts to fall, strong rays come from the Hobb's Lane and the received power increases by more than 25dB. When the trolley passes the crossing with Hobb's Lane, the power falls

again and remains low for the rest of the NLOS section of the route. The receiver re-enters the LOS area after the last corner, where the received power rises sharply.

The predictions were obtained using exactly the same simulation parameters as for Tx1 and Tx2. Again, the model manages to follow the measurements very closely for the majority of the receiver positions. The correct power levels have been predicted for the LOS and most of the NLOS sections of the route. The only divergence exists for the section of the route between the first and second corner. As mentioned before, it is believed that a possible explanation for the errors in this area may be some missing scatterers in the data base. Nevertheless, the problem is confined in a small region and the model follows the trend of the measurements for the rest of the route. With the values expressed in a linear scale and normalised to the measurements, the mean and the RMS errors are –3.9dB and 2dB, respectively. The mean error, calculated with both values in a logarithmic scale, is small, just -0.06dB, with an RMS error of 3.7dB.

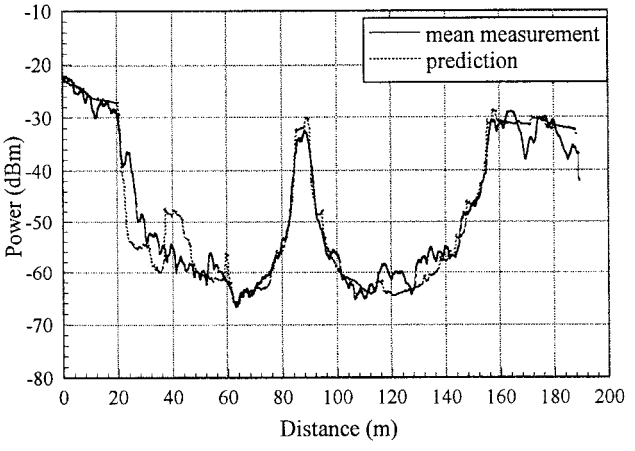

Figure 7: Model's prediction against mean measurement for transmitter position Tx3.

V. CONCLUSIONS

The paper has investigated the accuracy of narrowband predictions of a site specific urban propagation model in a microcellular environment. The comparisons with measurements for a typical highly cluttered city centre scenario showed that the predictions followed the trend of the measured power envelopes very well even in deeply shadowed areas. The mean errors were less than 1dB and the RMS errors did not exceed 3.7dB, for the different tests. These values indicate that the ray tracing model can achieve accurate microcellular predictions.

ACKNOWLEDGEMENTS

The narrowband measurements shown in this paper were performed by Dr S.A.Meade and Mr E.K.Tameh of the University of Bristol and funded by British Telecom as part of the Virtual University Research Initiative (VURI) project.

REFERENCES

[1] G.V.Tsoulos, G.E.Athanasiadou, M.A.Beach, S.C. Swales, "Adaptive Antennas for Microcellular and Mixed Cell Environments with DS-CDMA", *accepted for publication to the Wireless Personal Comms Journal, Kluwer Academic Publishers.*

[2] G.E.Athanasiadou, A.R.Nix, J.P.McGeehan, "A ray tracing algorithm for microcellular wideband propagation modelling", *IEEE VTC '95*, pp. 261-265, Chicago USA, 25-28 July 1995

[3] G.E.Athanasiadou, A.R.Nix, J.P.McGeehan, "A ray tracing algorithm for microcellular and indoor propagation modelling", *IEE ICAP '95*, pp. 2.231-2.235, Eindhoven Holland, 4-7 April 1995.

[4] J.W.McKnown and R.L.Hamilton, "Ray-tracing as a design tool for radio networks", *IEEE Networks Mag.*, pp. 21-26, Nov. 1991.

[5] M.C.Lawton, J.P.McGeehan, "The application of a deterministic ray launching algorithm for the prediction of radio channel characteristics in small-cell environments", *IEEE Trans. on Veh. Technol.*, vol. 43, no. 4, Nov. 1994.

[6] K. Rizk, A. Mawira, J-F Wagen, F. Cardiol, "Propagation with Urban Microcells with High Rise Buildings ", *IEEE VTC'96*, pp. 859-863, Atlanta, May 1996.

[7] G. Yang, K. Pahlavan, J.F. Lee, A.J. Dagen, J. Vancraeynest, "Prediction of Radio Wave Propagation in Four Blocks of New York City Using 3-D Ray Tracing", *IEEE PIMRC 1994*, A3.2, vol. I, pp. 263-267.

[8] K.R.Schaubach, N.J.Davis IV, "Microcellular radio-channel propagation prediction", *IEEE Antennas and Propag. Mag.*, pp.25-34, August 1994.

[9] S.A.Meade, A.R.Nix, M.A.Beach, "Summary of the Processing of the Narrowband Measurement Data for Microcells", University of Bristol, August 1996, Technical Report for the BT VURI project.

[10] G.E.Athanasiadou, A.R.Nix, J.P.McGeehan, "Indoor 3D Ray Tracing Predictions and their Comparison with High Resolution Wideband Measurements", *IEEE VTC'96*, Atlanta, USA, vol. 1, pp. 36-40, May 1996.